ACS APPLIED MATERIALS & INTERFACES

Research Article

Cite This: ACS Appl. Mater. Interfaces 2018, 10, 9164−9177

www.acsami.org

Interfacial Strength and Surface Damage Characteristics of Atomically Thin h-BN, MoS_2, and Graphene

Bien-Cuong Tran Khac,[†] Frank W. DelRio,[‡] and Koo-Hyun Chung*,[†]

[†]School of Mechanical Engineering, University of Ulsan, Ulsan 44610, Republic of Korea

[‡]Applied Chemicals and Materials Division, Material Measurement Laboratory, National Institute of Standards and Technology, Boulder, Colorado 80305, United States

Supporting Information

ABSTRACT: Surface damage characteristics of single- and multilayer hexagonal boron nitride (h-BN), molybdenum disulfide (MoS_2), and graphene films were systematically investigated via atomic force microscopy (AFM)-based progressive-force and constant-force scratch tests and Raman spectroscopy. The film-to-substrate interfacial strengths of these atomically thin films were assessed based on their critical forces (i.e., the normal force where the atomically thin film was delaminated from the underlying substrate), as determined from progressive-force scratch tests. The evolution of surface damage with respect to normal force was further investigated using constant-force tests. The results showed that single-layer h-BN, MoS_2, and graphene strongly adhere to the SiO_2 substrate, which significantly improves its tribological performance. Moreover, defect formation induced by scratch testing was found to affect the topography and friction force differently prior to failure, which points to distinct surface damage characteristics. Interestingly, the residual strains at scratched areas suggest that the scratch test-induced in-plane compressive strains were dominant over tensile strains, thereby leading to buckling in front of the scratching tip and eventually failure at sufficient strains. These trends represent the general failure mechanisms of atomically thin materials because of a scratch test. As the number of layers increased, the tribological performances of atomically thin h-BN, MoS_2, and graphene were found to significantly improve because of an increase in the interfacial strengths and a decrease in the surface damage and friction force. In all, the findings on the distinctive surface damage characteristics and general failure mechanisms are useful for the design of reliable, protective and solid-lubricant coating layers based on these materials for nanoscale devices.

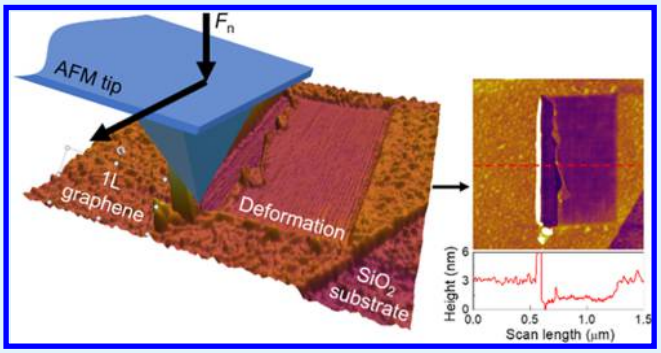

KEYWORDS: *surface damage, nanotribology, h-BN, MoS_2, graphene, nanoscratch test, atomic force microscopy (AFM)*

INTRODUCTION

Two-dimensional materials such as single- and multilayer h-BN, MoS_2, and graphene have attracted intensive interest because of their remarkable material properties. For instance, superior mechanical properties of these atomically thin films were recently found, in which the in-plane elastic moduli of single-layer h-BN, MoS_2, and graphene were determined to be about 865,[1] 270,[2] and 1000 GPa,[3] respectively. Low-friction characteristics of these atomically thin films were also observed in the literature, with friction coefficients ranging from 0.001 to 0.1,[4−7] which clearly demonstrate their potential for effective friction reduction at interfaces. Moreover, atomically thin h-BN, MoS_2, and graphene exhibit outstanding thermal stability up to more than 1000 °C[8−10] as well as phenomenal oxidation resistance.[11−13] Apart from material properties, the sub-nanometer thickness of single-layer h-BN, MoS_2, and graphene has made these materials of considerable interest for high-performance nanoscale devices, where the spacing between mechanical parts was extremely limited. Therefore, based on the outstanding material properties and atomic thicknesses, atomically thin h-BN, MoS_2, and graphene are useful as protective and solid-lubricant coating layers for nanoscale devices.[14]

To prolong the lifetime of high-performance nanoscale devices, protective and solid-lubricant coating layers are often used to improve tribological performances, including friction reduction, wear protection, and surface damage characteristics, at the contacting interfaces between the moving parts in the systems. Therefore, comprehensive investigations of the tribological performance and surface damage resistance of these thin films as protective and solid-lubricant coating layers are essential. In this regard, several studies have been conducted to assess wear resistance and surface damage protection of atomically thin h-BN,[15,16] MoS_2,[17] and graphene.[18−22] Although these studies generally demonstrated the potential of these layered materials in significantly reducing friction and

Received: January 1, 2018
Accepted: February 21, 2018
Published: February 21, 2018

DOI: 10.1021/acsami.8b00001
ACS Appl. Mater. Interfaces 2018, 10, 9164−9177

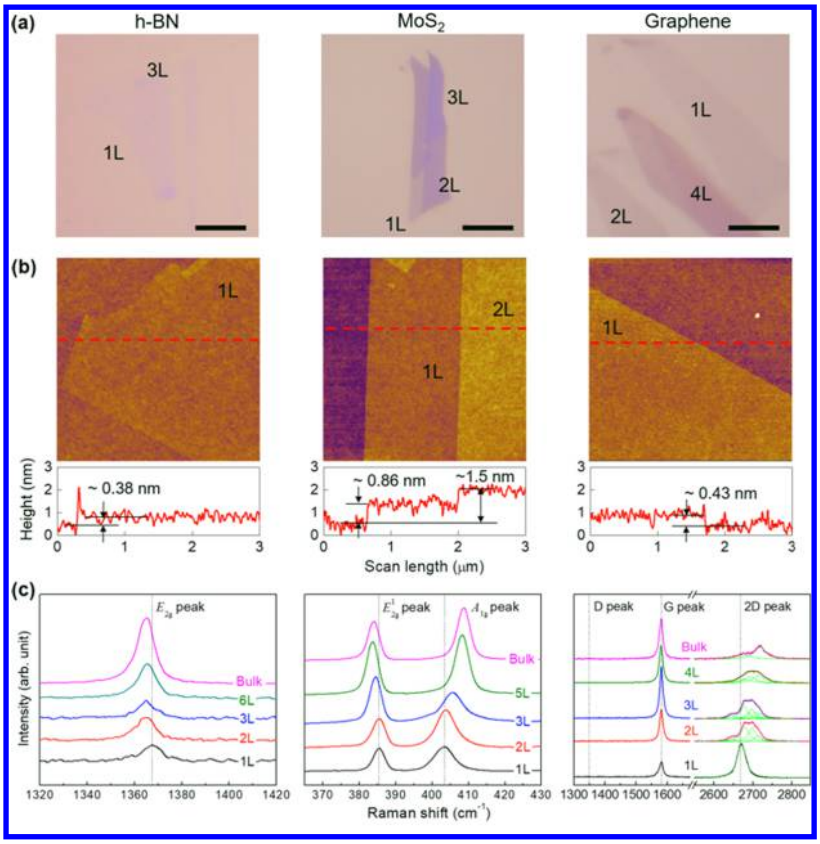

Figure 1. (a) Optical microscopy images, (b) topographic images, and (c) Raman spectra of single- and multilayer h-BN, MoS_2, and graphene. In (a), the scale bars are 5 μm. In (b), the cross-sectional profiles are included and the locations of these are indicated by red dashed lines. In (c), the frequencies of the characteristic peaks for single-layer h-BN, MoS_2, and graphene are denoted as dashed lines for comparison. 2D peaks in the Raman spectra of graphene were fitted with a Lorentzian equation.

wear in mechanical systems, the nanoscale surface damage characteristics and factors that could influence the tribological performance of atomically thin h-BN, MoS_2, and graphene specimens have not been clearly investigated. Particularly, given that the film-to-substrate interfacial strength significantly affects the tribological performance, few studies have systematically studied the interfacial strength of these atomically thin films. For instance, the interfacial strength of exfoliated and epitaxial graphene was studied as a function of the number of layers and was analyzed based on the observed critical force F_c (i.e., the normal force F_n where the atomically thin film delaminates from the substrate) from progressive-force scratch testing via a tribotester.[23] However, this study found that the critical forces for atomically thin graphene specimens were significantly scattered, even with the same number of layers.[23] Given that the tribological properties of these films depend so heavily on their interfacial strengths, an accurate and reliable determination of their critical forces is needed. In addition, failure of atomically thin graphene with plastic deformation of the underlying substrate was observed via scratch tests.[19,20] However, defect formation at the scratched areas was not fully analyzed, and given that defect formation can result in a significant degradation of mechanical strength in graphene,[24] the correlation between defects/damage and tribological performance must also be assessed. Finally, despite atomically thin h-BN and MoS_2 also being identified as good potential candidates for protective and solid-lubricant coating layers, even less is known about their tribological properties relative to graphene.

To practically implement atomically thin h-BN, MoS_2, and graphene as protective and solid-lubricant coating layers, scalable growth and deposition of high-quality atomically thin materials is highly desired. There are a number of studies on preparation methods for these materials such as epitaxial growth,[25,26] laser thinning,[27,28] physical vapor deposition,[29,30] and chemical vapor deposition (CVD).[22,31,32] Among these techniques, CVD methods have demonstrated the greatest potential for producing large-scale atomically thin films with the ability to precisely control the number of layers.[33] However, there are several problems related to crystalline quality, grain boundary structure, continuity, and scalability of CVD-grown films,[32,34] and as a result, CVD films often exhibit poor frictional behavior compared to pristine films via mechanical exfoliation. Recent efforts have focused on enhancing CVD film quality by optimizing the growth and deposition conditions using the frictional behavior of pristine materials as a guide.[35] Therefore, from a tribological viewpoint, a systematic investigation of interfacial strengths and surface damage characteristics for pristine atomically thin h-BN, MoS_2, and graphene will not only provide a fundamental understanding of the materials but also impart practical information for the development of CVD methods.

In this study, the film-to-substrate interfacial strengths and surface damage characteristics of atomically thin h-BN, MoS_2, and graphene were systematically investigated via atomic force microscopy (AFM)-based progressive-force and constant-force scratch tests. The diamond AFM tip used in the scratch tests was carefully calibrated in both normal and lateral directions to

DOI: 10.1021/acsami.8b00001
ACS Appl. Mater. Interfaces 2018, 10, 9164−9177

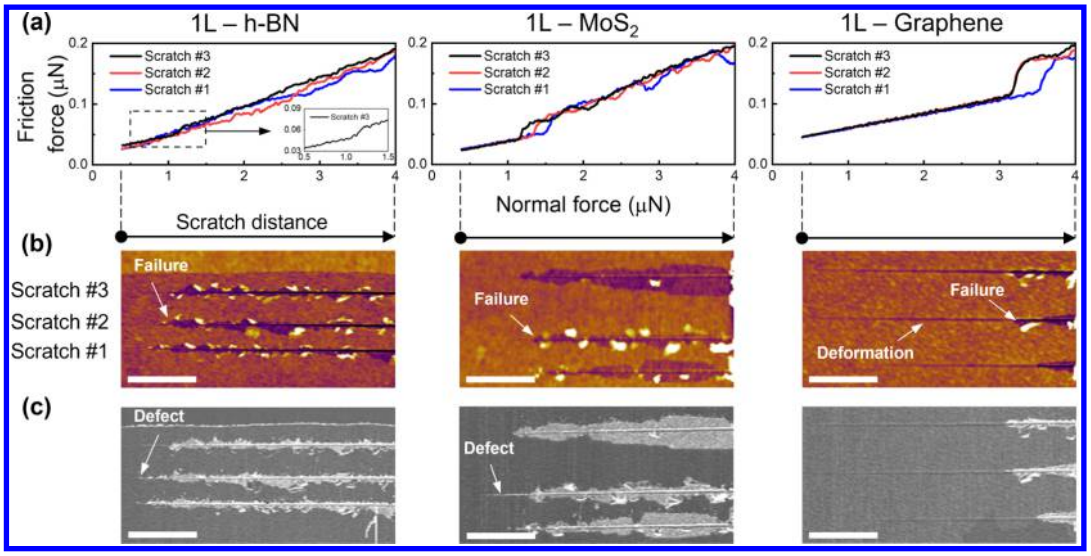

Figure 2. Progressive-force scratch test results for single-layer h-BN, MoS_2, and graphene specimens. (a) Friction force variation with respect to the normal force. The normal force was progressively increased from 400 to 4000 nN over a scratch distance of 2 μm. (b) Topographic and (c) FFM (forward scans) images of scratch tracks from single-layer h-BN, MoS_2, and graphene. The critical forces for the specimens were determined from the abrupt change in the friction force during the scratch test, where the failure of the specimens occurred and the substrate was exposed. In (b,c), the scale bars are 500 nm.

provide more accurate force measurements. Single- and multilayer h-BN, MoS_2, and graphene films mechanically exfoliated on SiO_2 substrates were carefully characterized using AFM and Raman spectroscopy prior to scratch tests. On the basis of the progressive-force scratch test results, the interfacial strengths of single-layer h-BN, MoS_2, and graphene were evaluated from the respective critical forces, all of which demonstrated that these atomically thin materials strongly adhere to the SiO_2 substrates. The constant-force scratch tests also showed the evolution of surface damage as a function of normal force and clearly revealed their distinctive surface damage characteristics induced by scratch testing. The commonly observed residual in-plane compressive strains at the scratched areas suggest a general failure mechanism. As the number of layers increased, the tribological properties (e.g., interfacial strength, friction force, and surface damage) of atomically thin h-BN, MoS_2, and graphene generally improved. It was shown that graphene was superior to h-BN and MoS_2 with regard to interfacial strength and surface damage characteristics. Overall, these findings provide a comprehensive understanding of the surface damage characteristics of h-BN, MoS_2, and graphene, which is critical to the development of these materials as protective and solid-lubricant coating layers for nanoscale devices.

RESULTS AND DISCUSSION

Specimen Characterization. Figure 1a shows the optical microscopy images of single- and multilayer h-BN, MoS_2, and graphene on SiO_2 substrates. The locations of single-layer MoS_2 and graphene specimens could be clearly identified based on their strong thickness-dependent optical contrast, whereas single-layer h-BN specimens were relatively difficult to observe because of their low optical contrast on SiO_2.[36] As the number of layers increased, the optical contrast increased, and single-layer h-BN specimens could be randomly located nearby thicker ones. Topographic images of the atomically thin specimens obtained from intermittent-contact mode AFM, as shown in Figure 1b, clearly demonstrate the relatively clean surfaces of these specimens. On the basis of the cross-sectional height profiles, single-layer h-BN, MoS_2, and graphene thicknesses were determined to be about 0.38, 0.86, and 0.43 nm, respectively, in good agreement with previous studies.[37−39] In addition, the variations in the thickness and surface roughness for single- and multilayer h-BN, MoS_2, and graphene with respect to the number of layers, as shown in Figure S1, clearly revealed the atomically thin and flat nature of these specimens.

Single- and multilayer h-BN, MoS_2, and graphene films were further examined by Raman spectroscopy with a 532 nm excitation source at room temperature. Raman spectra of atomically thin h-BN, MoS_2 and graphene specimens, as shown in Figure 1c, clearly show the dependence of their Raman characteristic peaks on the thickness, which is consistent with other studies.[36,40,41] Particularly, the Raman spectra of single-layer h-BN specimens show a relatively weak E_{2g} characteristic peak ($\approx$1367 cm^{-1}) from in-plane vibrations of B−N atoms.[36] As the number of layers increased, the intensity of the E_{2g} peak significantly increased and its frequency decreased (red-shifted). In the case of atomically thin MoS_2 specimens, their Raman spectra show two Raman characteristic peaks, the E^1_{2g} and A_{1g} peaks, which are associated with the in-plane vibrations of Mo−S atoms and the out-of-plane vibration of S atoms, respectively.[40] As the number of layers decreased, the frequency of the E^1_{2g} peak increased (blue-shifted), whereas that of the A_{1g} peak decreased (red-shifted). For the atomically thin graphene specimens, two Raman characteristic peaks including the G peak ($\approx$1580 cm^{-1}) and 2D peak ($\approx$2670 cm^{-1}) can be clearly observed from the Raman spectra. From the G peak and 2D peak, which result from the in-plane vibrations of the sp^2 carbon atoms and a two-phonon double resonance Raman process, respectively, the 2D peak was used to identify the number of graphene layers.[41] In particular, single-layer graphene shows a sharp and symmetric 2D peak, which can be fit by only one Lorentzian peak. As the thickness increases, the 2D peak becomes broader and the frequency increases

DOI: 10.1021/acsami.8b00001
ACS Appl. Mater. Interfaces 2018, 10, 9164−9177

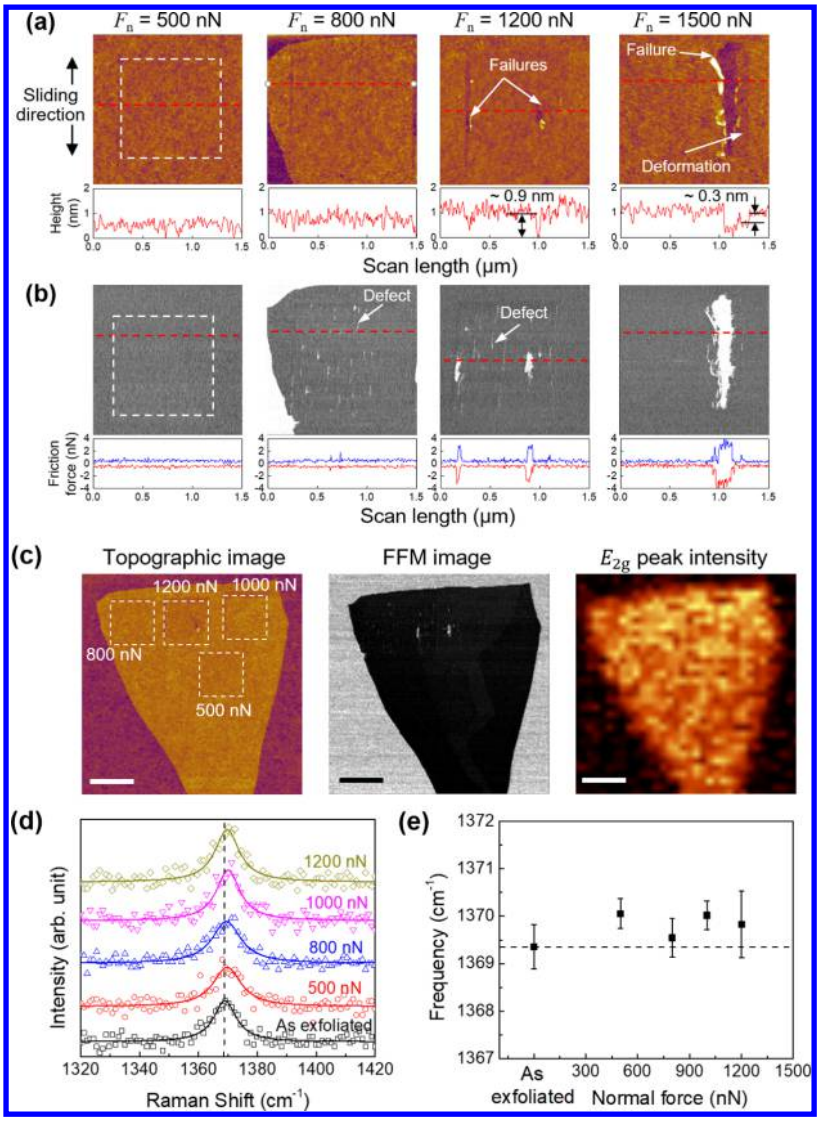

Figure 3. Topographic, FFM, and Raman intensity images of single-layer h-BN after constant-force scratch tests. High-resolution (a) topographic and (b) FFM (forward scan) images of single-layer h-BN after constant-force scratch tests at (from left to right) 500, 800, 1200, and 1500 nN normal force. (c) Topographic image, FFM image (forward scan), and Raman image for the E_{2g} peak intensity of single-layer h-BN after a constant-force scratch test at normal forces ranging from 500 to 1200 nN. (d) Raman spectra and (e) E_{2g} peak frequencies of scratched single-layer h-BN with respect to the normal force. The specimens were scratched at a constant normal force in the scratch area of 1 μm × 1 μm, as indicated by the white dashed squares in (a–c). The cross-sectional profiles and friction loops are included in (a,b), which demonstrate the change in friction and topographical characteristics of single-layer h-BN because of the constant-force scratch tests. In (c), the scale bars are 1 μm. The Raman spectra were fitted using a Lorentzian equation, and the frequency of the E_{2g} peak from the as-exfoliated single-layer h-BN is denoted as a dashed line in (d,e). Error bars represent 1 standard deviation of the mean.

(blue shifts), resulting in four Lorentzian peaks for bilayer graphene[41] and two Lorentzian peaks for graphite.[42]

Interfacial Strength of Single-Layer Materials. After characterization of the thickness of atomically thin h-BN, MoS_2, and graphene specimens using AFM and Raman spectroscopy, film-to-substrate interfacial strengths were evaluated based on their critical forces, as determined from progressive-force scratch tests. In previous studies, accurate and reliable determinations of critical forces for atomically thin films via scratch tests were difficult.[23,43] This study looks to address some of the issues by correlating the friction force variation with respect to normal force during progressive-force scratch tests with the topographic and friction force microscopy (FFM) images of the scratched areas. In this test, single-layer h-BN, MoS_2, and graphene specimens were scratched with a diamond AFM tip under normal forces progressively increasing from 400 to 4000 nN. The friction force variation with respect to normal force during the test was monitored as shown in Figure 2a, and the critical force was characterized by the normal load at which there was an abrupt increase in the friction force. Scratch tracks on the atomically thin specimens were clearly observed in the subsequent topographic and FFM images, as shown in Figure 2b,c, respectively. Topographic images of the scratched areas were obtained using relatively sharp Si AFM tips with a nominal tip radius of around 2 nm, which is roughly 20 times smaller than that of the diamond AFM tips used for the scratch tests (hence, the topography of scratched areas could be clearly observed). In addition, FFM images from only the forward scan directions were included for clarity, where the darker contrast indicates lower friction and brighter contrast indicates higher

DOI: 10.1021/acsami.8b00001
ACS Appl. Mater. Interfaces 2018, 10, 9164–9177

friction. Given that the friction force of SiO_2 is significantly larger than those of the atomically thin specimens, the failure of the latter could be observed in the FFM images. On the basis of these observations, the critical forces for single-layer h-BN, MoS_2, and graphene were determined to be about 900 ± 200, 1300 ± 150, and 3300 ± 200 nN, respectively, which correspond to contact pressures of 4.33, 7.14, and 8.15 GPa, respectively. It is important to specify that these contact pressures were estimated using the Derjaguin−Muller−Toporov (DMT) contact model, in which the attractive forces between the AFM tip and SiO_2 substrate are predominantly outside the contact area[44] and represent a convolution of both the film and substrate properties. These critical contact pressures clearly demonstrate a significant improvement in the load-carrying capacity of the SiO_2 substrate, as provided by single-layer h-BN, MoS_2, and graphene, given that the compressive strength of thermally grown amorphous SiO_2 is only between 0.69 and 1.38 GPa.[45] Furthermore, the results indicate that single-layer graphene has the largest critical force, followed by single-layer MoS_2 and h-BN, which suggests that single-layer graphene may have the largest interfacial strength. However, it is important to note that the critical forces could also be strongly influenced by the mechanical properties of the respective film.[23] For example, breaking strengths of single-layer h-BN, MoS_2, and graphene have been reported to be about 23,[1] 15,[2] and 42 N/m,[3] respectively. The significantly smaller strengths of single-layer h-BN and MoS_2 as compared to single-layer graphene could result in less mechanical stability during the scratch test.[46] In other words, single-layer h-BN and MoS_2 could be more easily deformed, whereas single-layer graphene could effectively endure more normal force. Thus, even though single-layer h-BN and MoS_2 are generally good as solid lubricants, their relatively weak interfacial strengths could significantly degrade their tribological performances.

From the topographic images in Figure 2b, single-layer h-BN and MoS_2 specimens were found to tear off and expose the substrate, shortly after scratch tracks were observed on the top surface. Furthermore, as shown in the corresponding FFM images in Figure 2c, the scratch tracks exhibited an increase in friction just prior to failure, which indicates that defects were likely formed at the scratch tracks. Interestingly, in the case of single-layer graphene, a height decrease at the scratch tracks with increasing F_n was observed prior to the failure of the specimens, as shown in Figure 2b. However, the FFM image in Figure 2c shows that the scratch tracks of graphene maintained their low frictional behavior until failure occurred. This behavior suggests that the underlying SiO_2 substrate was plastically deformed by the scratch test, but given the superior mechanical strength of graphene, the film remained intact up until failure. The out-of-plane bending of the films is likely responsible for the deformation of the underlying substrate. In more detail, the bending moduli of single-layer h-BN, MoS_2 and graphene have been reported to be about 0.95,[47] 9.61,[48] and 1.40 eV,[49] respectively. The relatively large out-of-plane bending modulus for single-layer MoS_2 could be responsible for the fact that no significant plastic deformation was observed in the underlying substrate in the single-layer MoS_2 scratch tracks. Interestingly, there was also limited plastic deformation of the substrate at the scratch tracks of the single-layer h-BN, despite its small bending modulus. In this case, the plastic deformation of the substrate might occur either simultaneously with or shortly before the failure of the specimen because of the relatively low mechanical strength and high sensitivity to shear stress of single-layer h-BN.[46]

On the basis of the critical forces from the progressive-force tests, the film-to-substrate interfacial strengths of single-layer h-BN, MoS_2, and graphene specimens were evaluated. In general, the results show that these atomically thin films strongly adhere to the SiO_2 substrates, which in turn significantly improve the load-carrying capacity of the substrate. In addition, the surface damage characteristics of the films prior to failure (e.g., defect formation and plastic deformation) were significantly different. To gain a better understanding of the surface damage characteristics of single-layer h-BN, MoS_2, and graphene, constant-force scratch tests were performed.

Surface Damage Characteristics of Single-Layer Materials. In the constant-force scratch tests, a diamond tip was used to scratch a defined area of 1 μm × 1 μm on the surface of the specimens under given normal forces, with the overarching goal to observe the evolution of surface damage with respect to normal force. The scratched areas were carefully characterized by AFM and Raman spectroscopy measurements. Topographic images with cross-sectional profiles and FFM images with friction loops of scratched areas on single-layer h-BN specimens under various normal forces are shown in Figure 3a,b, respectively. On the basis of the AFM and FFM data, no significant changes in topography and friction were observed at the scratched area under 500 nN normal force. As the normal force increased to 800 nN, although no significant change was observed in the topographic image, a few spikes with a higher friction force were locally observed along the scratch direction in the FFM image, which indicates that a few surface defects were likely formed at the scratched area. These defects were observed in FFM images of the scratched area under 1200 nN normal force. In addition, local failures were observed in both the AFM and FFM images of the scratched area under 1200 nN normal force, suggesting that this load was sufficient to delaminate the film and expose the underlying substrate. The single-layer h-BN eventually failed at 1500 nN normal force (≈5.09 GPa contact pressure). Shortly before the failure of the specimens, a small height decrease of about 0.3 nm was observed at the scratched area, whereas its friction force was not significantly changed. This behavior may be attributed to the plastic deformation of the underlying SiO_2 substrate, whereas the single-layer h-BN remained intact for a few scratches.

Surface damage characteristics of scratched areas were further investigated using Raman spectroscopy. Figure 3c shows the topographic and FFM images and the corresponding Raman intensity map of the E_{2g} peak (≈1370 cm^{-1}) for a single-layer h-BN specimen after scratch testing at normal forces ranging from 500 to 1200 nN. As shown in the figure, defect formation and failure can be observed in the topographic and FFM images but without significant changes to the E_{2g} peak intensity. The results suggest that the E_{2g} peak intensity may not be affected by the defects. This behavior is similar to that of the G peak in defective graphene, where its intensity is not significantly influenced by defects.[50] It should be noted that both the E_{2g} peak of h-BN and the G peak of graphene originate from the E_{2g} phonon mode, which is the in-plane vibrational mode of the B−N atoms and C atoms, respectively.[36]

Figure 3d,e shows the Raman spectra and E_{2g} peak frequencies from scratched areas under various normal forces, respectively. The spectra show that the E_{2g} frequency at scratched areas increased by 0.3−0.8 cm^{-1} as compared to that

DOI: 10.1021/acsami.8b00001
ACS Appl. Mater. Interfaces 2018, 10, 9164−9177

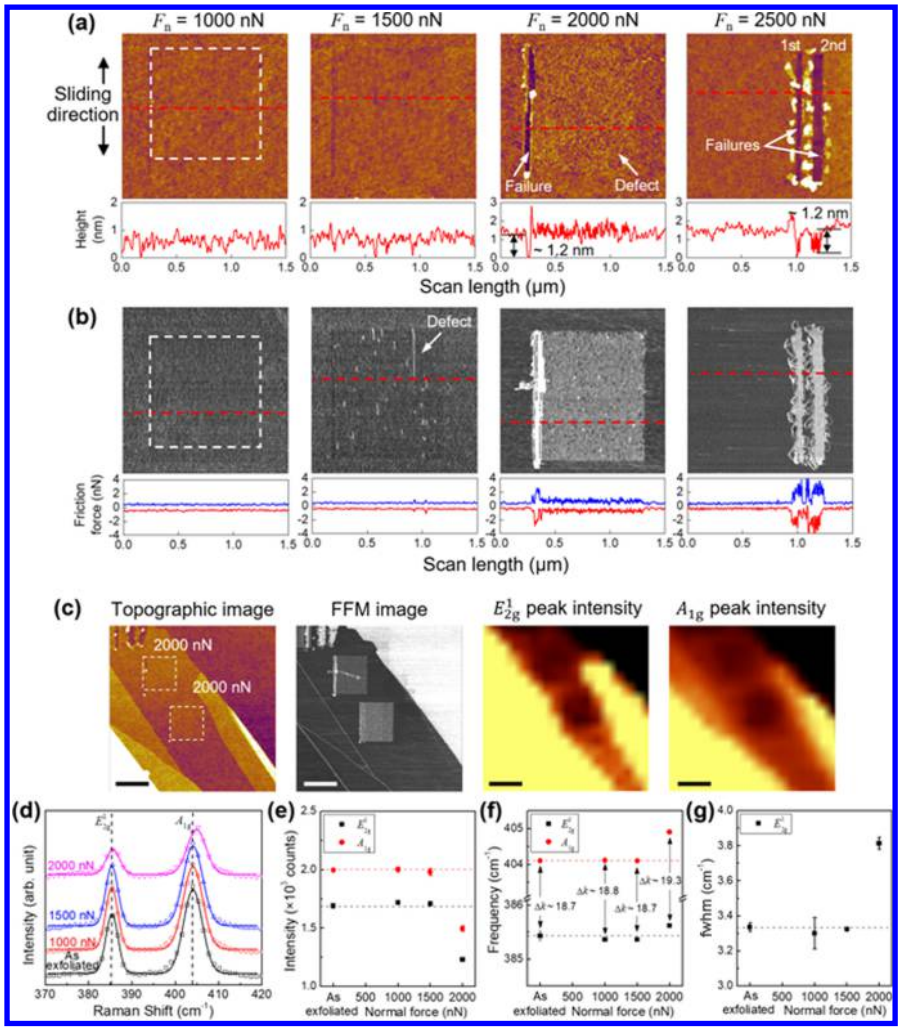

Figure 4. Topographic, FFM, and Raman intensity images of single-layer MoS_2 after constant-force scratch tests. High-resolution (a) topographic and (b) FFM (forward scan) images of single-layer MoS_2 after constant-force scratch tests at (from left to right) 1000, 1500, 2000, and 2500 nN normal force. (c) Topographic image, FFM image (forward scan), and Raman images for the E^1_{2g} and A_{1g} peak intensities of single-layer MoS_2 after a constant-force scratch test at a normal force of 2000 nN. (d) Raman spectra and E^1_{2g} and A_{1g} (e) intensities and (f) frequencies of scratched single-layer MoS_2 with respect to the normal force. (g) Raman E^1_{2g} peak fwhm of scratched single-layer MoS_2 with respect to the normal force. The specimens were scratched at a constant normal force in the scratch area of 1 μm × 1 μm, as indicated by the white dashed squares in (a–c). The cross-sectional profiles and friction loops are included in (a,b), which demonstrate the change in friction and topographical characteristics of single-layer MoS_2 because of the constant-force scratch tests. In (c), the scale bars are 1 μm. The Raman spectra were fitted with a Gaussian equation, and the intensity and frequency of the E^1_{2g} and A_{1g} peaks from the as-exfoliated single-layer MoS_2 are denoted as dashed lines in (d–f). The E^1_{2g} peak fwhm from the as-exfoliated single-layer MoS_2 is also denoted by a dashed line in (g). Error bars represents 1 standard deviation of the mean.

of as-exfoliated specimens. In general, compressive strain produces phonon hardening and tensile strain produces phonon softening, which results in blue-shifting and red-shifting of the corresponding Raman mode, respectively.[31] Therefore, the observed blue shift of the E_{2g} peak is feasibly due to in-plane compressive strain at the scratched areas induced by the scratch tests. Interestingly, although no significant change was observed from both the topographic and FFM images of the scratched area under 500 nN normal force, the Raman spectrum obtained from this area shows a blue shift of ≈0.8 cm^{-1} for the E_{2g} peak, which indicates that there may be a certain degree of compressive strain in the layer. As the normal force increased from 500 to 1200 nN, the blue shift of the E_{2g} peak in the scratched areas was relatively constant, which implies that the amount of compressive strain was also constant. It is speculated that the degree of strain in the scratched areas should increase as the normal force increases but that the defect formation and local failure relieves some of this strain, giving the appearance that accumulated strain is independent of the normal force. The defect formation on the surface of single-layer h-BN might have originated from pure mechanical failure from broken bonds generated by local penetration of the AFM tip or the formation of tetrahedron with three B atoms in the plane because of the out-of-plane deformation of the N atom during the scratch testing, considering that broken bond and tetrahedron defects were shown to have the smallest formation energies.[51]

Figure 4a,b shows the topographic and FFM images of single-layer MoS_2 specimens after constant-force scratch tests at various normal forces, respectively. At 1000 nN normal force, no significant damage of specimens was observed in both the topographic and FFM images. As the normal force increased to 1500 nN, several spikes with higher friction were locally observed in the FFM image but without accompanying changes

DOI: 10.1021/acsami.8b00001
ACS Appl. Mater. Interfaces 2018, 10, 9164–9177

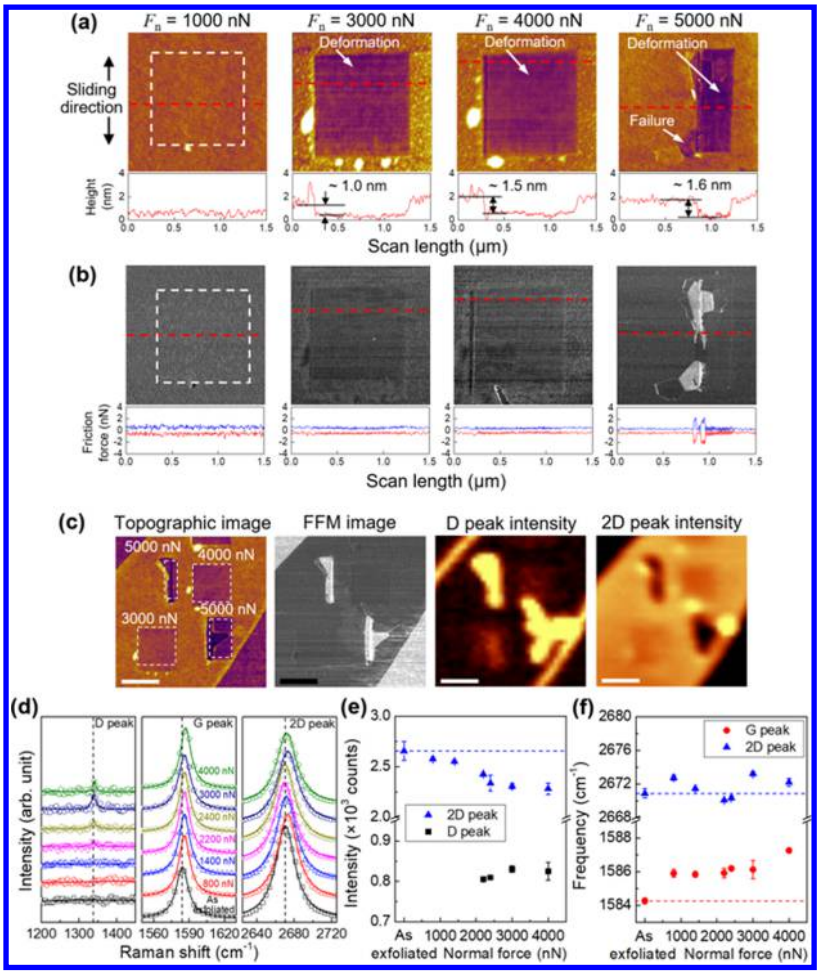

Figure 5. Topographic, FFM, and Raman intensity images of single-layer graphene after constant-force scratch tests. High-resolution (a) topographic and (b) FFM (forward scan) images of single-layer graphene after constant-force scratch tests at (from left to right) 1000, 3000, 4000, and 5000 nN normal force. (c) Topographic image, FFM image (forward scan), and Raman images for the D and 2D peak intensities of single layer graphene after a constant-force scratch test at normal forces ranging from 3000 to 5000 nN. (d) Raman spectra and D, G, and 2D (e) intensities and (f) frequencies of scratched single-layer graphene with respect to the normal force. The specimens were scratched at a constant normal force in the scratch area of 1 μm × 1 μm, as indicated by the white dashed squares in (a–c). The cross-sectional profiles and friction loops are included in (a,b), which demonstrate the change in friction and topographical characteristics of single-layer graphene because of the constant-force scratch tests. In (c), the scale bars are 1 μm. The Raman spectra were fitted with a Lorentzian equation, and the intensity and frequency of the G and 2D peaks from the as-exfoliated single-layer graphene are denoted as dashed lines in (d–f). Error bars represent 1 standard deviation of the mean.

in the topographic image. These observations indicate that a few defects were formed on the surface of the scratched area and resulted in increasing friction force at those areas. Both surface roughness and friction force were found to significantly increase at 2000 nN normal force, although the specimen was not yet removed from the substrate. The increase in roughness and friction was likely due to the formation of additional defects in the specimen. Interestingly, at the end of the 2000 nN test, complete failure of the single-layer MoS_2 specimen was observed, with the removal of the film from the substrate. This observation suggests that the maximum contact pressure that single-layer MoS_2 can endure just prior to failure is ≈8.21 GPa. At 2500 nN normal force, single-layer MoS_2 was found to immediately delaminate from SiO_2.

Figure 4c shows the topographic and FFM images and the corresponding Raman intensity maps of the E^1_{2g} and A_{1g} peaks for a single-layer MoS_2 specimen after scratch tests at 2000 nN normal force. On the basis of the topographic and FFM images, defect formation on the surface was clearly observed. The corresponding Raman intensity maps of the E^1_{2g} and A_{1g} peaks clearly show darker contrast at the scratched areas compared to the as-exfoliated areas, which indicates that the intensities of the E^1_{2g} and A_{1g} peaks at the scratched areas were lower than those from the as-exfoliated areas. As shown in Figure 4d,e, the E^1_{2g} and A_{1g} peak intensities exhibit this abrupt decrease after scratch testing at 2000 nN normal force. Raman spectra and peak frequencies from scratched areas at various normal forces also show a blue shift of the E^1_{2g} and A_{1g} peaks at 2000 nN normal force relative to the as-exfoliated areas, as illustrated in Figure 4d,f. The decrease in the intensity and the increase in the frequency of the E^1_{2g} peak may indicate in-plane compressive strains, whereas those of the A_{1g} peak may be due to out-of-plane compressive strains at scratched areas under 2000 nN normal force.[40,52] By contrast, the intensities and frequencies at smaller F_n were not significantly altered, which suggest that the compressive strain in the layer was relatively small after the scratch tests.

The crystalline quality of the single-layer MoS_2 specimens after the scratch tests was further characterized by Raman spectroscopy based on the frequency separation between the

DOI: 10.1021/acsami.8b00001
ACS Appl. Mater. Interfaces 2018, 10, 9164–9177

E^1_{2g} and A_{1g} peaks, Δk, and the full width at half-maximum (fwhm) of the E^1_{2g} peak.[32,34] Δk and E^1_{2g} fwhm were obtained from the Raman spectra, as shown in Figure 4f,g, respectively. The values of Δk for single-layer MoS_2 specimens after scratch testing at 1000 and 1500 nN normal force were found to be about 18.8 and 18.7 cm^{-1}, respectively, which is close to that from as-exfoliated areas (≈18.7 cm^{-1}). The E^1_{2g} fwhm values for single-layer MoS_2 specimens after scratch testing at 1000 and 1500 nN normal force were found to be around 3.30 and 3.32 cm^{-1}, respectively, which also agree with that from as-exfoliated areas (≈3.34 cm^{-1}). Together, the results indicate that single-layer MoS_2 specimens can sustain good crystalline quality after scratch tests up to 1500 nN. However, the values for Δk and E^1_{2g} fwhm at 2000 nN were determined to be about 19.3 and 3.81 cm^{-1}, respectively, significantly larger than those from as-exfoliated areas. Thus, the quality has greatly degraded at this contact pressure,[32,34] likely due to the formation of defects.

In general, surface defects of atomically thin MoS_2 can occur from different surface treatment conditions. Such defects include particle adsorption on the surface from high-power laser treatment,[39] oxygen chemical adsorption at crack sites because of high-temperature annealing,[53] and wrinkle formation on the surface because of a combination of compressive stress and shear.[54] In this study, the defects that formed at scratched areas are likely due to the formation of wrinkles on the surface. In more detail, single-layer MoS_2 was compressed and wrinkled ahead of the tip as it moved across the surface, resulting in the observed changes to roughness and friction. The wrinkle formation on the surface of single-layer MoS_2 is similar to what was observed in multilayer MoS_2.[54] It should be noted that Barboza et al. suggested that such wrinkle formation can only be observed in multilayer MoS_2, given that their single-layer MoS_2 specimens did not exhibit this behavior at normal loads from 10 to 391 nN. However, it is now apparent that wrinkle formation can occur, albeit at much larger forces (2000 nN) and contact pressures (8.21 GPa). It is possible that the high temperatures generated at the contacting interface between the AFM tip and specimen could also cause the formation of Mo−O bonding because of oxygen chemical adsorption.[53] However, based on the Raman spectra obtained from the scratched areas, the oxidation of MoS_2 is not likely to occur because of the absence of a Raman peak at 820 cm^{-1}, which is the Raman signature for oxidized MoS_2.[28,55] Furthermore, chemically adsorbed oxygen has been reported to provide a significant photoluminescence enhancement in single-layer MoS_2.[53] However, based on the results in Figure S2, it is clear that there is a significant decrease in photoluminescence at scratched areas under 2000 nN normal force, providing further evidence that single-layer MoS_2 is not oxidized during the scratch testing.

Figure 5a,b shows the topographic and FFM images of single-layer graphene specimens after constant-force scratch tests at various normal forces, respectively. On the basis of the AFM images, no significant change was observed in the topography at the scratched area under a normal force of 1000 nN. A height decrease of about 1.0 nm was observed in the topographic image at 3000 nN normal force. As the normal force increased from 4000 to 5000 nN, the height decreased from 1.5 to 1.6 nm, respectively, prior to failure. Interestingly, no significant changes in the frictional behavior were observed at any of the scratched areas. These behaviors indicate that the SiO_2 substrate was plastically deformed because of the large contact pressure induced by the scratch tests, and the degree of plastic deformation increased as the normal force increased. The maintained low friction force at the scratched areas shows that single-layer graphene specimens could endure the scratch test and cover the plastically deformed substrate up to 5000 nN normal force (9.34 GPa contact pressure).

Figures S3 and 5c show the topographic and FFM images and the corresponding Raman intensity maps of the D and 2D peaks for single-layer graphene after the constant-force scratch tests at normal forces from 800 to 2400 nN and from 3000 to 5000 nN, respectively. The D peak (≈1350 cm^{-1}) corresponds to the breathing mode of six-atom rings and is only activated by defects.[41] Although no defect is required for the activation of the 2D peak, its intensity is also strongly influenced by defects.[56] Hence, on the basis of the changes in the intensities of the D and 2D peaks after scratch testing, defect formation was clearly observed. As shown in the AFM images, the topography started to change because of plastic deformation of the substrate after scratch tests at 1400 nN normal force (6.17 GPa contact pressure). As the normal force increased, the degree of plastic deformation in the substrate increased, which in turn changed the topography of the single-layer graphene. By contrast, no significant changes in the friction force were observed. From the D and 2D peak Raman maps, where brighter (darker) contrast represents higher (lower) intensity, defect formation was clearly observed. A significant number of defects were observed at the edges of the single-layer graphene, as expected.[41]

Raman spectra of the D, G, and 2D regions at scratched areas under various normal forces are shown in Figure 5d. From these spectra, it was possible to extract both the peak intensity and frequency as a function of the normal force, as shown in Figure 5e,f. The Tuinstra−Koenig relation was employed[57] with the intensity data in Figure 5e to estimate the defect density at the scratched areas

$$L_D = [2.4 \times 10^{-10}\ \mathrm{nm}^{-3}]\lambda^4 (I_D/I_G)^{-1}$$

where L_D is the distance between pointlike defects, λ is the Raman excitation wavelength (≈532 nm), and I_D/I_G is the intensity ratio of the D and G peaks.[58,59] At normal forces of 2200 and 4000 nN, the intensity ratio I_D/I_G was determined to be about 0.45 and 0.48, respectively. Hence, on the basis of the Tuinstra−Koenig relation, the distances between defects formed at the scratched areas were estimated to be about 42.22 and 40.82 nm, respectively. This suggests that as the normal force increased, the density of the defects at the scratched areas increased slightly. Interestingly, the estimated values of L_D suggest that the scratched areas in this study have a relatively low defect density as compared to previous studies ($L_D \geq 10$ nm).[58,60] From the nanoindentation results of single-layer graphene using molecular dynamic simulations, it was shown that right after failure, cracks in the graphene effectively healed, resulting in a few small defects at the failure site.[21] The relatively low-defect density in the scratched graphene could be responsible for the lack of changes to the friction force.

The frequency data for scratched single-layer graphene at various normal forces are shown in Figure 5f. As the normal force increases, the data clearly demonstrate that the G peak blue shifts and the 2D peak remain unchanged. The blue shift in the G peak is likely attributed to the in-plane compressive strain in the single-layer graphene specimens at the scratched areas.[61] The G peak frequency increases as the normal force increases, which suggests that the degree of in-plane compressive strain also increases. Finally, it is important to

DOI: 10.1021/acsami.8b00001
ACS Appl. Mater. Interfaces 2018, 10, 9164−9177

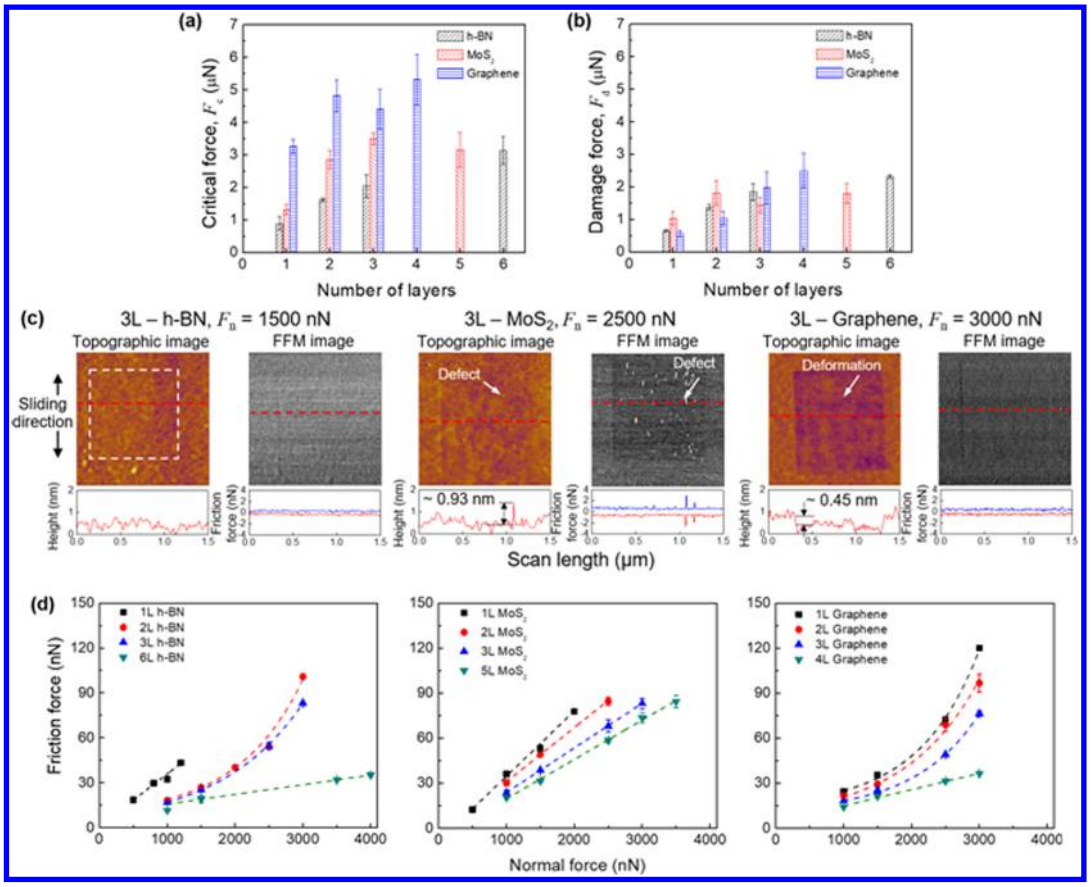

Figure 6. (a) Critical force and (b) damage force for single- and multilayer h-BN, MoS_2, and graphene. (c) High-resolution topographic and FFM (forward scan) images of trilayer h-BN, MoS_2, and graphene after a constant-force scratch test. (d) Friction force as a function of the normal force for single- and multilayer h-BN, MoS_2, and graphene. The specimens were scratched at a constant normal force in the scratch area of 1 μm × 1 μm, as indicated by the white dashed squares in (c). The cross-sectional profiles and friction loops are also included in (c), which demonstrate the change in friction and topographical characteristics because of the constant-force scratch tests. Error bars represent 1 standard deviation of the mean.

note that the G peak blue shifts at normal forces as low as 800 nN, despite no observable changes to topography and friction. This behavior is similar to that of single-layer h-BN after being scratched at 500 nN normal force.

From a Raman study on graphite, a three-stage classification of disorder along an amorphization trajectory ranging from graphite to tetrahedral amorphous carbon (ta-C) was proposed: (1) graphite to nanocrystalline graphite, (2) nanocrystalline graphite to amorphous carbon (a-C, ≈20% sp^3); and (3) a-C to ta-C (>85% sp^3).[62] In our study, on the basis of the Raman spectra of the D and G peaks obtained at the scratched areas with respect to normal force, stage 1 is likely the most relevant.[60] In this stage, which represents the transformation from single-crystal graphene to nanocrystalline graphene from scratch tests under 4000 nN normal force, the evolution of the Raman spectra is as follows:[60,62] (1) D peak appeared and the intensity ratio I_D/I_G increased, (2) G peak frequency increased, and (3) G peak showed no dispersion. It is well-known that pristine single-crystal graphene is extraordinary in terms of its mechanical toughness and strength but also that defective nanocrystalline graphene experiences significant degradation in these properties.[24] Thus, it is also possible that defect formation could potentially affect its tribological performance as a protective and solid-lubricant coating layer. For instance, the pre-existing defects at the edges of the film could be the reason that a much small normal force (2 orders of magnitude) was required to cause failure at the graphene edge as compared to the graphene interior area.[20]

In total, the constant-force scratch tests suggest that the evolution of surface damage for single-layer h-BN, MoS_2, and graphene can be defined via a multistage layer removal process: (1) elastic deformation, (2) defect formation and propagation in the film and/or plastic deformation of the film-substrate system, and (3) total removal of the film from the underlying substrate. At stage (1), the atomically thin specimens remained intact with no significant defect formation after scratch tests under relatively small normal forces. In this stage, the films provide their best tribological performance for extended periods of time, despite the presence of residual in-plane compressive strains, as observed from Raman measurements of the scratched areas. Interestingly, previous work at small F_n has shown that the films may wrinkle in the region beneath the tip, but that the original planar structure of the materials is eventually restored after the tip passes, resulting in a reversible negative compressibility effect.[54] At stage (2), as F_n increased, defects in the film and plastic deformation of the substrate were noted. Although failure had not yet occurred, the topography, friction force, and crystalline quality of single-layer h-BN, MoS_2, and graphene were permanently affected, leading to the potential degradation of their tribological performances. The irreversible wrinkles observed in this study at these intermediate F_n values are likely due to local fracture events at the folds. At $F_n \geq F_c$ (stage 3), atomically thin films were

DOI: 10.1021/acsami.8b00001
ACS Appl. Mater. Interfaces 2018, 10, 9164–9177

torn off and the substrates were exposed, likely due to the compressive strain induced by the tip during the scratch tests. In general, compressive and tensile strains occur simultaneously during the scratch test, with compressive stress originating ahead of the tip and tensile stress induced behind the tip, as shown in Figure S4. However, a recent study on single-layer graphene has established an asymmetry in its mechanical instability: the critical compressive strain for buckling is markedly smaller than the critical tensile strain for fracture. In more detail, the compressive strain to buckling was found to be $\approx 10^{-4}$%, whereas the tensile strain for fracture was ≈2%.[63] Such an asymmetry is expected for most two-dimensional materials and suggests that these atomically thin specimens are particularly susceptible to compressive strains.[64] Under compression, two types of mechanical instabilities are induced: buckling and fracture. The compressive strains initially buckle the film, but as the normal force increases, it will eventually lead to rupture of the atomic bonds.[21,64] This multistage process denotes the general failure mechanism in single-layer h-BN, MoS_2, and graphene specimens subjected to scratch testing.

Interfacial Strength and Surface Damage Characteristics of Multilayer Materials. It has been proposed that multilayer graphene provides better tribological characteristics than single-layer graphene.[19] However, the mechanism for this enhancement has not yet been clearly explained. To elucidate this mechanism, we investigate the interfacial strength and surface damage characteristics of multilayer h-BN, MoS_2, and graphene. The friction force variation with respect to normal force during progressive-force scratch tests and the corresponding topographic and FFM images of scratched areas for multilayer h-BN, MoS_2, and graphene are shown in Figures S5a−c, S6a−c, and S7a−c, respectively. Together with the single-layer results, the critical forces F_c were assessed and summarized with respect to number of layers, as demonstrated in Figure 6a. The result clearly shows that as the number of layers increased, the critical forces generally increased, which indicates that the film-to-substrate interfacial strengths generally increased with the number of layers. This behavior may be partly attributed to the van der Waals interactions of the substrate not only with its nearest layer but also with other layers in the multilayer film.

The high-resolution topographic and FFM images for scratch tracks on single- and multilayer h-BN, MoS_2, and graphene are shown in Figures S5d,e, S6d,e, and S7d,e, respectively. The topographic images clearly show the failure of single- and multilayer h-BN and MoS_2 specimens along with exposure of the SiO_2 substrate relatively shortly after the formation of scratch tracks on the top surface. Furthermore, shortly prior to failure, an increase in friction was also observed, which is likely due to defect formation. Interestingly, the formation of defects at the scratch tracks affected the topography of the h-BN and MoS_2 specimens differently. For instance, for trilayer h-BN under 1400 nN normal force, a height decrease of ≈1.0 nm was clearly observed at the first scratch track in Figure S5d. By contrast, a height increase of ≈2.1 nm was observed at the second scratch track on trilayer MoS_2 at 3000 nN normal force, as shown in Figure S6d. The behavior of graphene is similar to that of h-BN; bilayer graphene exhibited a height decrease of ≈0.5 nm under 3000 nN normal force, as shown in Figure S7d. As previously discussed, the height decrease for h-BN and graphene is likely due to plastic deformation of the substrate, whereas the height increase for MoS_2 is likely due to wrinkle formation on the film. The overall behavior for the multilayer films is consistent with what was observed from the single-layer specimens.

The normal force required to induce surface damage such as plastic deformation and wrinkle formation was also characterized with respect to the number of layers. By definition, the force required to induce damage, F_d, is less than or equal to the critical force required to delaminate the film from the underlying substrate, F_c. As shown in Figure 6b, F_d generally increased with the number of layers for h-BN, MoS_2, and graphene. For layered materials subjected to indentation tests, the thicker the specimen is, the harder it is to deform,[1,2] which is likely due to an increase in the bending modulus with the number of layers. Thus, as the number of h-BN and graphene layers increased, the normal force to induce plastic deformation of the substrate also increased. For atomically thin MoS_2, out-of-plane bending was minimized because of its relatively large bending stiffness, and as such, the failure mechanism changed to that of wrinkling and folding of the top layer. The onset of these wrinkling and folding phenomena was directly related to the number of layers (i.e., there was a delayed occurrence as the number of layers increased), which suggest that the binding energy between the top layer and its lower layers may increase with increasing number of layers. This behavior is in agreement with a previous study,[65] which proposed that the amount of energy needed to peel off the top layer significantly increased as the number of underlying layers increased because of the enhanced interlayer binding energy that the top layer received when the material became thicker. In all, the progressive scratch test results on h-BN, MoS_2, and graphene showed an increase in the interfacial strength and a decrease in the surface damage for a given F_n, as the number of layers increased.

Constant-force scratch tests were also conducted on h-BN, MoS_2, and graphene multilayer specimens. Topographic and FFM images of scratched areas on trilayer h-BN, MoS_2, and graphene under various normal forces clearly show that surface damage via wrinkle formation and plastic deformation was reduced as the number of layers increased, as shown in Figure 6c. For instance, at 1500 nN normal force, single-layer h-BN was torn from the substrate after only a few scratches, whereas no significant damage was observed in the scratched area of trilayer h-BN. Similarly, single-layer MoS_2 immediately failed at 2500 nN normal force, whereas just a few wrinkles were locally formed in the scratched areas of trilayer MoS_2. For graphene at 3000 nN normal force, a height decrease of about 0.5 nm was observed for trilayer graphene, whereas a height decrease of 1 nm was found at scratched areas in single-layer graphene at the same force. The result indicates that the degree of plastic deformation in the substrate at the scratched areas of trilayer graphene was significantly reduced.

The friction forces from the constant-force scratch tests are plotted with respect to the number of layers in Figure 6d, which clearly shows thickness-dependent friction behavior for h-BN, MoS_2, and graphene. At the same normal force, friction force was found to increase as the number of layers decreased, resulting in the largest friction for single-layer specimens. The dependence of friction force on the number of layers is a general trend for these layered materials[66] and has been attributed to the out-of-plane deformation or "puckering" of the top layers in front of the AFM tip during contact sliding. Interestingly, the thickness-dependent friction was observed in this study in the presence of wrinkle formation and plastic deformation at very large normal forces, whereas these phenomena were likely eliminated in the study of Lee et al.[66]

DOI: 10.1021/acsami.8b00001
ACS Appl. Mater. Interfaces 2018, 10, 9164−9177

at very small normal forces (≈1 nN with tip radius of about 10 nm). In addition, it has been shown here that two very different frictional behaviors are possible depending on the composition and thickness of the specimen: a linear and nonlinear dependence of friction force on the normal force. In more detail, MoS_2 (regardless of number of layers), single- and hexalayer h-BN, and tetralayer graphene clearly demonstrate a linear relationship with the normal force, whereas bi- and trilayer h-BN and single-, bi, and trilayer graphene show a nonlinear dependence of friction force on the normal force. On the basis of the topographic images of the films after scratch tests, as shown in Figure S8, we found that the linear and nonlinear dependences of friction force on the normal force is closely related to the deformation of the underlying SiO_2 substrate. The close correlation between plastic deformation at the scratched areas and nonlinear dependence of friction force on normal force suggests that the deformation of the substrate introduces additional friction force to the AFM tip during scratch tests. This additional friction force is likely attributed to the shear force required to plow the underlying SiO_2 substrate at the scratched areas. In a recent study on the friction characteristics between a silica probe and micelle layers,[67] the authors also observed an additional friction force due to the deformation of the micelle layers, resulting in the nonlinear dependence of friction force on the normal force. As the number of layers increased, the deformation of the substrate at scratched areas was effectively reduced. Hence, the friction force of hexalayer h-BN and tetralayer graphene specimens during scratch tests remained linearly proportional to the normal force, as clearly shown in Figure 6d.

CONCLUSIONS

In summary, this study presents a systematical investigation of the interfacial strength and surface damage characteristics for single- and multilayer h-BN, MoS_2, and graphene via AFM-based progressive-force and constant-force scratch tests. The film-to-substrate interfacial strengths were evaluated based on their critical forces obtained from the progressive-force scratch tests. The results suggest that these atomically thin films strongly adhered to the substrates, which significantly improved its load-carrying capacity. For single-layer films, graphene was found to have a larger interfacial strength than h-BN and MoS_2.

The surface damage characteristics of h-BN, MoS_2, and graphene specimens were further investigated via constant-force scratch tests. The results suggest three different steps in the evolution of surface damage. At relatively low normal force, no significant change in the topography and friction force was observed, which points to elastic deformation in the scratched area. As the normal force increased, the formation of defects in the film and plastic deformation in the substrate was noted. At this stage, although the films have not yet failed, their topography, friction force, crystalline quality, and mechanical strengths are affected, which notably degrade their tribological performance. At $F_n \geq F_c$, delamination of the film from the substrate occurs. The residual in-plane compressive strain observed from the scratched areas of single- and multilayer h-BN, MoS_2, and graphene specimens further elucidated the failure mechanism. The compressive strain-induced buckling in front of the tip was the primary source of mechanical instability. As the compressive strain increased, the atomic bonds were compressed and eventually ruptured.

The improvements to interfacial strength, surface damage resistance, and friction characteristics indicate that the tribological performance could be effectively enhanced by simply increasing the thickness of the specimens. However, these increases in the thickness could come at the expense of other desired features, such as electrical properties. Therefore, it is essential to use a film thickness that optimizes the properties for the application of interest.

MATERIALS AND METHODS

Single- and multilayer h-BN, MoS_2, and graphene specimens were produced from high-quality single-crystal h-BN (HQ Graphene), MoS_2 (SPI Supplies), and graphite (NGS), respectively, via micromechanical exfoliation.[68] These atomically thin materials were repeatedly exfoliated from their bulk crystals using an adhesive tape. The freshly exfoliated atomically thin materials on the tape were then gently pressed against and transferred to a Si wafer capped with a 300 nm-thick thermally grown SiO_2 layer. Up to hexalayer h-BN, pentalayer MoS_2, and tetralayer graphene were prepared with an aim to investigate the interfacial strength and surface damage as a function of the number of layers. Optical microscopy (VK-X200, Keyence), AFM (MFP-3D, Asylum Research), and Raman spectroscopy (Alpha300R, Witec) were employed to carefully examine the topography and thickness of the atomically thin specimens prior to scratch tests. In more detail, the atomically thin films were first located using optical microscopy. Topographic data were then obtained via intermittent-contact mode AFM using Si probes with a nominal spring constant of 2 N/m (AC240, Olympus). Raman spectroscopy measurements were performed using an excitation laser wavelength of 532 nm. Raman spectra were collected through a 100× objective (NA ≈ 0.9) with a laser spot size of about 720 nm, and the spectra resolution was set to be about 1.4 cm^{-1} (1800 lines/mm grating). The laser power was kept below 0.5 mW with an acquisition time of 10 s to eliminate laser-induced thermal effects[69] and particle formation[39] on the specimens.

After sample preparation and characterization, the interfacial strength and surface damage characteristics of the films were investigated via AFM-based progressive and constant-force scratch tests. A nanocrystalline diamond tip (NaDiaProbes, Advanced Diamond Technologies) with a tip radius of about 40 nm was used in both the progressive-force and constant-force tests. For the quantitative determination of the normal and friction forces, the cantilevers were calibrated in both normal[70] and lateral[71,72] directions. On the basis of the force calibration results, the normal spring constant and lateral sensitivity of the diamond probe used for scratch tests were about 45 N/m and 0.02 mV/nN, respectively. The sliding speed of the diamond tip was set to 500 nm/s for both tests.

In the progressive-force scratch test, single-layer h-BN, MoS_2, and graphene specimens were scratched under a progressive normal force for one single scratch line with the scratch distance of 2 μm. First, the diamond tip was brought into contact with the specimens at a relatively low normal force of 400 nN to keep the tip stable on the specimen surface.[20] Once contact was established, the specimen was scratched under a normal force that was progressively increased from 400 to 4000 nN to find the critical force of the specimen. As noted earlier, the critical force is defined as the normal force, where the atomically thin specimens were removed and the substrate was exposed.[23] The critical force was resolved via three to five sets of progressive-force scratch tests. The progressive-force tests were also performed with multilayer h-BN, MoS_2, and graphene to investigate the effects of film thickness on the interfacial strength and surface damage.

In the constant-force scratch test, single-layer h-BN, MoS_2, and graphene specimens were scratched in a defined area of 1 μm × 1 μm under a constant normal force. In each area, the specimens were scratched at a given normal force ranging from 500 to 5000 nN to observe the evolution of surface damage on single-layer specimens with respect to the normal force. The adhesion force between the AFM tip and the specimens were carefully tracked during all scratch tests to monitor tip wear (Figure S9).[73] The contact pressure between the AFM tip and specimen was estimated by the DMT contact model,

DOI: 10.1021/acsami.8b00001
ACS Appl. Mater. Interfaces 2018, 10, 9164−9177

which includes the effects of the adhesive forces outside the area of contact.[44]

After the scratch tests, the topography and frictional behaviors of the scratched areas were investigated via intermittent-contact mode AFM and contact mode AFM. In the intermittent-contact mode, relatively sharp Si tips with a nominal tip radius of about 2 nm (SuperSharpSilicon, NANOSENSORS) were used for imaging. FFM images were obtained in the contact mode using Si tips with a nominal spring constant of 0.2 N/m (LFMR,NANOSENSORS). On the basis of the force calibration results, the normal spring constant and lateral sensitivity of the Si tips used for FFM imaging ranged from 0.37 to 0.47 N/m and from 3.0 to 5.9 mV/nN, respectively. The normal force was set to 0.5 nN to observe the frictional behavior of the scratched areas without introducing additional damage to the specimens. The scratched areas were also characterized using Raman intensity mapping. The Raman intensity images were obtained by scanning the specimens with a laser step size of 230 nm and an acquisition time of 0.5−1.0 s for each spectrum. All experiments were conducted under ambient conditions (25 °C, 30% relative humidity).

■ ASSOCIATED CONTENT

Supporting Information

The Supporting Information is available free of charge on the ACS Publications website at DOI: 10.1021/acsami.8b00001.

Additional results from AFM, FFM, Raman, and photoluminescence measurements (PDF)

■ AUTHOR INFORMATION

Corresponding Author

*E-mail: khchung@ulsan.ac.kr. Phone: +82-52-259-2744. Fax: +82-52-259-1680.

ORCID

Bien-Cuong Tran Khac: 0000-0001-9710-4276

Frank W. DelRio: 0000-0003-1727-8220

Koo-Hyun Chung: 0000-0002-9092-6784

Author Contributions

The manuscript was written through contributions made by all authors. All authors have approved the final version of the manuscript.

Notes

The authors declare no competing financial interest.

■ ACKNOWLEDGMENTS

K.-H.C. acknowledges the financial support from the University of Ulsan by the 2016 research fund. F.W.D. recognizes the support from the National Institute of Standards and Technology. Certain commercial equipment, instruments, or materials are identified to specify the experimental procedure adequately. The identification is not intended to imply recommendation or endorsement by NIST, nor is it intended to imply the materials or equipment identified are necessarily the best available for the purpose. This is a partial contribution of NIST, not subject to copyright in the United States.

■ REFERENCES

(1) Falin, A.; Cai, Q.; Santos, E. J. G.; Scullion, D.; Qian, D.; Zhang, R.; Yang, Z.; Huang, S.; Watanabe, K.; Taniguchi, T.; Barnett, M. R.; Chen, Y.; Ruoff, R. S.; Li, L. H. Mechanical Properties of Atomically Thin Boron Nitride and the Role of Interlayer Interactions. *Nat. Commun.* **2017**, *8*, 15815.

(2) Bertolazzi, S.; Brivio, J.; Kis, A. Stretching and Breaking of Ultrathin MoS_2. *ACS Nano* **2011**, *5*, 9703−9709.

(3) Lee, C.; Wei, X.; Kysar, J. W.; Hone, J. Measurement of the Elastic Properties and Intrinsic Strength of Monolayer Graphene. *Science* **2008**, *321*, 385−388.

(4) An, X.; Yao, H.; Ma, F.; Lu, Z. The Influence of Electronic Transfer on Friction Properties of Hexagonal Boron Nitride. *RSC Adv.* **2015**, *5*, 106239−106244.

(5) Ataca, C.; Ciraci, S. Functionalization of Single-Layer MoS_2 Honeycomb Structures. *J. Phys. Chem. C* **2011**, *115*, 13303−13311.

(6) Filleter, T.; McChesney, J. L.; Bostwick, A.; Rotenberg, E.; Emtsev, K. V.; Seyller, T.; Horn, K.; Bennewitz, R. Friction and Dissipation in Epitaxial Graphene Films. *Phys. Rev. Lett.* **2009**, *102*, 086102.

(7) Saito, T.; Honda, F. Chemical Contribution to Friction Behavior of Sintered Hexagonal Boron Nitride in Water. *Wear* **2000**, *237*, 253−260.

(8) Kostoglou, N.; Polychronopoulou, K.; Rebholz, C. Thermal and Chemical Stability of Hexagonal Boron Nitride (h-BN) Nanoplatelets. *Vacuum* **2015**, *112*, 42−45.

(9) Radisavljevic, B.; Radenovic, A.; Brivio, J.; Giacometti, V.; Kis, A. Single-layer MoS_2 Transistors. *Nat. Nanotechnol.* **2011**, *6*, 147−150.

(10) Kim, K.; Regan, W.; Geng, B.; Alemán, B.; Kessler, B. M.; Wang, F.; Crommie, M. F.; Zettl, A. High-Temperature Stability of Suspended Single-layer Graphene. *Phys. Status Solidi RRL* **2010**, *4*, 302−304.

(11) Chen, S.; Brown, L.; Levendorf, M.; Cai, W.; Ju, S.-J.; Edgeworth, J.; Li, X.; Magnuson, C. W.; Velamakanni, A.; Piner, R. D.; Kang, J.; Park, J.; Ruoff, R. S. Oxidation Resistance of Graphene-coated Cu and Cu/Ni Alloy. *ACS Nano* **2011**, *5*, 1321−1327.

(12) Li, L. H.; Cervenka, J.; Watanabe, K.; Taniguchi, T.; Chen, Y. Strong Oxidation Resistance of Atomically Thin Boron Nitride Nanosheets. *ACS Nano* **2014**, *8*, 1457−1462.

(13) Sen, H. S.; Sahin, H.; Peeters, F. M.; Durgun, E. Monolayers of MoS_2 as an Oxidation Protective Nanocoating Material. *J. Appl. Phys.* **2014**, *116*, 083508.

(14) Spear, J. C.; Ewers, B. W.; Batteas, J. D. 2D-nanomaterials for Controlling Friction and Wear at Interfaces. *Nano Today* **2015**, *10*, 301−314.

(15) Lee, B.; Lee, D.; Lee, J. H.; Ryu, H. J.; Hong, S. H. Enhancement of Toughness and Wear Resistance in Boron Nitride Nanoplatelet (BNNP) Reinforced Si_3N_4 Nanocomposites. *Sci. Rep.* **2016**, *6*, 27609.

(16) Cho, D.-H.; Kim, J.-S.; Kwon, S.-H.; Lee, C.; Lee, Y.-Z. Evaluation of Hexagonal Boron Nitride Nano-sheets as a Lubricant Additive in Water. *Wear* **2013**, *302*, 981−986.

(17) Hao, R.; Tedstone, A. A.; Lewis, D. J.; Warrens, C. P.; West, K. R.; Howard, P.; Gaemers, S.; Dillon, S. J.; O'Brien, P. Property Self-Optimization During Wear of MoS_2. *ACS Appl. Mater. Interfaces* **2017**, *9*, 1953−1958.

(18) Marchetto, D.; Held, C.; Hausen, F.; Wählisch, F.; Dienwiebel, M.; Bennewitz, R. Friction and Wear on Single-Layer Epitaxial Graphene in Multi-Asperity Contacts. *Tribol. Lett.* **2012**, *48*, 77−82.

(19) Vasić, B.; Matković, A.; Ralević, U.; Belić, M.; Gajić, R. Nanoscale Wear of Graphene and Wear Protection by Graphene. *Carbon* **2017**, *120*, 137−144.

(20) Qi, Y.; Liu, J.; Zhang, J.; Dong, Y.; Li, Q. Wear Resistance Limited by Step Edge Failure: The Rise and Fall of Graphene as an Atomically Thin Lubricating Material. *ACS Appl. Mater. Interfaces* **2016**, *9*, 1099−1106.

(21) Klemenz, A.; Pastewka, L.; Balakrishna, S. G.; Caron, A.; Bennewitz, R.; Moseler, M. Atomic Scale Mechanisms of Friction Reduction and Wear Protection by Graphene. *Nano Lett.* **2014**, *14*, 7145−7152.

(22) Kim, K.-S.; Lee, H.-J.; Lee, C.; Lee, S.-K.; Jang, H.; Ahn, J.-H.; Kim, J.-H.; Lee, H.-J. Chemical Vapor Deposition-Grown Graphene: The Thinnest Solid Lubricant. *ACS Nano* **2011**, *5*, 5107−5114.

(23) Shin, Y. J.; Stromberg, R.; Nay, R.; Huang, H.; Wee, A. T. S.; Yang, H.; Bhatia, C. S. Frictional Characteristics of Exfoliated and Epitaxial Graphene. *Carbon* **2011**, *49*, 4070−4073.

DOI: 10.1021/acsami.8b00001
ACS Appl. Mater. Interfaces 2018, 10, 9164−9177

(24) Shekhawat, A.; Ritchie, R. O. Toughness and Strength of Nanocrystalline Graphene. *Nat. Commun.* **2016**, *7*, 10546.
(25) Virojanadara, C.; Syväjarvi, M.; Yakimova, R.; Johansson, L. I.; Zakharov, A. A.; Balasubramanian, T. Homogeneous Large-area Graphene Layer Growth on 6H-SiC (0001). *Phys. Rev. B: Condens. Matter Mater. Phys.* **2008**, *78*, 245403.
(26) Dumcenco, D.; Ovchinnikov, D.; Marinov, K.; Lazić, P.; Gibertini, M.; Marzari, N.; Sanchez, O. L.; Kung, Y.-C.; Krasnozhon, D.; Chen, M.-W.; Bertolazzi, S.; Gillet, P.; Fontcuberta i Morral, A.; Radenovic, A.; Kis, A. Large-Area Epitaxial Monolayer MoS_2. *ACS Nano* **2015**, *9*, 4611−4620.
(27) Han, G. H.; Chae, S. J.; Kim, E. S.; Güneş, F.; Lee, I. H.; Lee, S. W.; Lee, S. Y.; Lim, S. C.; Jeong, H. K.; Jeong, M. S.; Lee, Y. H. Laser Thinning for Monolayer Graphene Formation: Heat Sink and Interference Effect. *ACS Nano* **2011**, *5*, 263−268.
(28) Castellanos-Gomez, A.; Barkelid, M.; Goossens, A. M.; Calado, V. E.; van der Zant, H. S. J.; Steele, G. A. Laser-Thinning of MoS_2: On Demand Generation of a Single-Layer Semiconductor. *Nano Lett.* **2012**, *12*, 3187−3192.
(29) Helveg, S.; Lauritsen, J. V.; Lægsgaard, E.; Stensgaard, I.; Nørskov, J. K.; Clausen, B. S.; Topsøe, H.; Besenbacher, F. Atomic-Scale Structure of Single-Layer MoS_2 Nanoclusters. *Phys. Rev. Lett.* **2000**, *84*, 951−954.
(30) Garlow, J. A.; Barrett, L. K.; Wu, L.; Kisslinger, K.; Zhu, Y.; Pulecio, J. F. Large-Area Growth of Turbostratic Graphene on Ni (111) via Physical Vapor Deposition. *Sci. Rep.* **2016**, *6*, 19804.
(31) Song, L.; Ci, L.; Lu, H.; Sorokin, P. B.; Jin, C.; Ni, J.; Kvashnin, A. G.; Kvashnin, D. G.; Lou, J.; Yakobson, B. I.; Ajayan, P. M. Large Scale Growth and Characterization of Atomic Hexagonal Boron Nitride Layers. *Nano Lett.* **2010**, *10*, 3209−3215.
(32) Zhan, Y.; Liu, Z.; Najmaei, S.; Ajayan, P. M.; Lou, J. Large-Area Vapor-Phase Growth and Characterization of MoS_2 Atomic Layers on a SiO_2 Substrate. *Small* **2012**, *8*, 966−971.
(33) Choi, H.; Lim, Y.; Park, M.; Lee, S.; Kang, Y.; Kim, M. S.; Kim, J.; Jeon, M. Precise Control of Chemical Vapor Deposition Graphene Layer Thickness using Ni_xCu_{1-x} Alloys. *J. Mater. Chem. C* **2015**, *3*, 1463−1467.
(34) Yu, Y.; Li, C.; Liu, Y.; Su, L.; Zhang, Y.; Cao, L. Controlled Scalable Synthesis of Uniform, High-Quality Monolayer and Few-layer MoS_2 Films. *Sci. Rep.* **2013**, *3*, 1866.
(35) Ky, D. L. C.; Khac, B.-C. T.; Le, C. T.; Kim, Y. S.; Chung, K.-H. Friction Characteristics of Mechanically Exfoliated and CVD-grown Single-layer MoS_2. *Friction* **2018**, DOI: 10.1007/s40544-017-0172-8.
(36) Gorbachev, R. V.; Riaz, I.; Nair, R. R.; Jalil, R.; Britnell, L.; Belle, B. D.; Hill, E. W.; Novoselov, K. S.; Watanabe, K.; Taniguchi, T.; Geim, A. K.; Blake, P. Hunting for Monolayer Boron Nitride: Optical and Raman Signatures. *Small* **2011**, *7*, 465−468.
(37) Kim, G.; Jang, A.-R.; Jeong, H. Y.; Lee, Z.; Kang, D. J.; Shin, H. S. Growth of High-Crystalline, Single-Layer Hexagonal Boron Nitride on Recyclable Platinum Foil. *Nano Lett.* **2013**, *13*, 1834−1839.
(38) Shearer, C. J.; Slattery, A. D.; Stapleton, A. J.; Shapter, J. G.; Gibson, C. T. Accurate Thickness Measurement of Graphene. *Nanotechnology* **2016**, *27*, 125704.
(39) Khac, B. C. T.; Jeon, K.-J.; Choi, S. T.; Kim, Y. S.; DelRio, F. W.; Chung, K.-H. Laser-Induced Particle Adsorption on Atomically Thin MoS_2. *ACS Appl. Mater. Interfaces* **2016**, *8*, 2974−2984.
(40) Li, H.; Zhang, Q.; Yap, C. C. R.; Tay, B. K.; Edwin, T. H. T.; Olivier, A.; Baillargeat, D. From Bulk to Monolayer MoS_2: Evolution of Raman Scattering. *Adv. Funct. Mater.* **2012**, *22*, 1385−1390.
(41) Ferrari, A. C.; Meyer, J. C.; Scardaci, V.; Casiraghi, C.; Lazzeri, M.; Mauri, F.; Piscanec, S.; Jiang, D.; Novoselov, K. S.; Roth, S.; Geim, A. K. Raman Spectrum of Graphene and Graphene Layers. *Phys. Rev. Lett.* **2006**, *97*, 187401.
(42) Vidano, R. P.; Fischbach, D. B.; Willis, L. J.; Loehr, T. M. Observation of Raman Band Shifting with Excitation Wavelength for Carbons and Graphites. *Solid State Commun.* **1981**, *39*, 341−344.
(43) Ollivier, B.; Matthews, A. Adhesion of Diamond-like Carbon Films on Polymers: an Assessment of the Validity of the Scratch Test Technique applied to Flexible Substrates. *J. Adhes. Sci. Technol.* **1994**, *8*, 651−662.
(44) Derjaguin, B. V.; Muller, V. M.; Toporov, Y. P. Effect of Contact Deformations on the Adhesion of Particles. *J. Colloid Interface Sci.* **1975**, *53*, 314−326.
(45) Morozov, O.; Postnikov, A. Mechanical Strength Study of SiO_2 Isolation Blocks Merged in Silicon Substrate. *J. Micromech. Microeng.* **2014**, *25*, 015014.
(46) Singh, S. K.; Neek-Amal, M.; Costamagna, S.; Peeters, F. M. Thermomechanical Properties of a Single Hexagonal Boron Nitride Sheet. *Phys. Rev. B: Condens. Matter Mater. Phys.* **2013**, *87*, 184106.
(47) Wu, J.; Wang, B.; Wei, Y.; Yang, R.; Dresselhaus, M. Mechanics and Mechanically Tunable Band Gap in Single-Layer Hexagonal Boron-Nitride. *Mater. Res. Lett.* **2013**, *1*, 200−206.
(48) Jiang, J.-W.; Qi, Z.; Park, H. S.; Rabczuk, T. Elastic Bending Modulus of Single-layer Molybdenum Disulfide (MoS_2): Finite Thickness Effect. *Nanotechnology* **2013**, *24*, 435705.
(49) Lu, Q.; Arroyo, M.; Huang, R. Elastic Bending Modulus of Monolayer Graphene. *J. Phys. D: Appl. Phys.* **2009**, *42*, 102002.
(50) Ahlberg, P.; Johansson, F. O. L.; Zhang, Z.-B.; Jansson, U.; Zhang, S.-L.; Lindblad, A.; Nyberg, T. Defect Formation in Graphene during Low-energy Ion Bombardment. *APL Mater.* **2016**, *4*, 046104.
(51) Slotman, G. J.; Fasolino, A. Structure, Stability and Defects of Single Layer Hexagonal BN in Comparison to Graphene. *J. Phys.: Condens. Matter* **2012**, *25*, 045009.
(52) Nayak, A. P.; Pandey, T.; Voiry, D.; Liu, J.; Moran, S. T.; Sharma, A.; Tan, C.; Chen, C.-H.; Li, L.-H.; Chhowalla, M.; Lin, J.-F.; Singh, A. K.; Akinwande, D. Pressure-Dependent Optical and Vibrational Properties of Monolayer Molybdenum Disulfide. *Nano Lett.* **2014**, *15*, 346−353.
(53) Nan, H.; Wang, Z.; Wang, W.; Liang, Z.; Lu, Y.; Chen, Q.; He, D.; Tan, P.; Miao, F.; Wang, X.; Wang, J.; Ni, Z. Strong Photoluminescence Enhancement of MoS_2 through Defect Engineering and Oxygen Bonding. *ACS Nano* **2014**, *8*, 5738−5745.
(54) Barboza, A. P. M.; Chacham, H.; Oliveira, C. K.; Fernandes, T. F. D.; Ferreira, E. H. M.; Archanjo, B. S.; Batista, R. J. C.; de Oliveira, A. B.; Neves, B. R. A. Dynamic Negative Compressibility of Few-Layer Graphene, h-BN, and MoS_2. *Nano Lett.* **2012**, *12*, 2313−2317.
(55) Windom, B. C.; Sawyer, W. G.; Hahn, D. W. A Raman Spectroscopic Study of MoS_2 and MoO_3: Applications to Tribological Systems. *Tribol. Lett.* **2011**, *42*, 301−310.
(56) Childres, I.; Jauregui, L. A.; Chen, Y. P. Raman Spectra and Electron-phonon Coupling in Disordered Graphene with Gate-tunable Doping. *J. Appl. Phys.* **2014**, *116*, 233101.
(57) Tuinstra, F.; Koenig, J. L. Raman Spectrum of Graphite. *J. Chem. Phys.* **1970**, *53*, 1126−1130.
(58) Lucchese, M. M.; Stavale, F.; Ferreira, E. H. M.; Vilani, C.; Moutinho, M. V. O.; Capaz, R. B.; Achete, C. A.; Jorio, A. Quantifying Ion-induced Defects and Raman Relaxation Length in Graphene. *Carbon* **2010**, *48*, 1592−1597.
(59) Chen, J.-H.; Cullen, W. G.; Jang, C.; Fuhrer, M. S.; Williams, E. D. Defect Scattering in Graphene. *Phys. Rev. Lett.* **2009**, *102*, 236805.
(60) Cançado, L. G.; Jorio, A.; Ferreira, E. H. M.; Stavale, F.; Achete, C. A.; Capaz, R. B.; Moutinho, M. V. O.; Lombardo, A.; Kulmala, T. S.; Ferrari, A. C. Quantifying Defects in Graphene via Raman Spectroscopy at Different Excitation Energies. *Nano Lett.* **2011**, *11*, 3190−3196.
(61) Proctor, J. E.; Gregoryanz, E.; Novoselov, K. S.; Lotya, M.; Coleman, J. N.; Halsall, M. P. High-pressure Raman Spectroscopy of Graphene. *Phys. Rev. B: Condens. Matter Mater. Phys.* **2009**, *80*, 073408.
(62) Ferrari, A. C.; Robertson, J. Interpretation of Raman Spectra of Disordered and Amorphous Carbon. *Phys. Rev. B: Condens. Matter Mater. Phys.* **2000**, *61*, 14095−14107.
(63) Zhang, Y.; Liu, F. Maximum Asymmetry in Strain Induced Mechanical Instability of Graphene: Compression versus Tension. *Appl. Phys. Lett.* **2011**, *99*, 241908.
(64) Peng, Q.; De, S. Outstanding Mechanical Properties of Monolayer MoS_2 and its Application in Elastic Energy Storage. *Phys. Chem. Chem. Phys.* **2013**, *15*, 19427−19437.

DOI: 10.1021/acsami.8b00001
ACS Appl. Mater. Interfaces 2018, 10, 9164−9177

(65) Björkman, T.; Gulans, A.; Krasheninnikov, A. V.; Nieminen, R. M. van der Waals Bonding in Layered Compounds from Advanced Density-Functional First-Principles Calculations. *Phys. Rev. Lett.* **2012**, *108*, 235502.
(66) Lee, C.; Li, Q.; Kalb, W.; Liu, X. Z.; Berger, H.; Carpick, R. W.; Hone, J. Frictional Characteristics of Atomically Thin Sheets. *Science* **2010**, *328*, 76−80.
(67) Li, J.; Luo, J. Nonlinear Frictional Energy Dissipation between Silica-Adsorbed Surfactant Micelles. *J. Phys. Chem. Lett.* **2017**, *8*, 2258−2262.
(68) Novoselov, K. S.; Geim, A. K.; Morozov, S. V.; Jiang, D.; Zhang, Y.; Dubonos, S. V.; Grigorieva, I. V.; Firsov, A. A. Electric Field Effect in Atomically Thin Carbon Films. *Science* **2004**, *306*, 666−669.
(69) Najmaei, S.; Liu, Z.; Ajayan, P. M.; Lou, J. Thermal Effects on the Characteristic Raman Spectrum of Molybdenum Disulfide (MoS_2) of Varying Thicknesses. *Appl. Phys. Lett.* **2012**, *100*, 013106.
(70) Hutter, J. L.; Bechhoefer, J. Calibration of Atomic-force Microscope Tips. *Rev. Sci. Instrum.* **1993**, *64*, 1868−1873.
(71) Khac, B. C. T.; Chung, K.-H. Quantitative Assessment of Contact and Non-contact Lateral Force Calibration Methods for Atomic Force Microscopy. *Ultramicroscopy* **2016**, *161*, 41−50.
(72) Chung, K.-H.; Reitsma, M. G. Note: Lateral Force Microscope Calibration using Multiple Location Pivot Loading of Rectangular Cantilevers. *Rev. Sci. Instrum.* **2010**, *81*, 026104.
(73) Chung, K.-H. Wear Characteristics of Atomic Force Microscopy Tips: A Review. *Int. J. Precis. Eng. Man.* **2014**, *15*, 2219−2230.

DOI: 10.1021/acsami.8b00001
ACS Appl. Mater. Interfaces 2018, 10, 9164−9177